nature nanotechnology

ARTICLES

PUBLISHED ONLINE: 16 OCTOBER 2011 | DOI: 10.1038/NNANO.2011.164

Nanochannel electroporation delivers precise amounts of biomolecules into living cells

Pouyan E. Boukany[1,2], Andrew Morss[1,3], Wei-ching Liao[1,4], Brian Henslee[1,2], HyunChul Jung[5], Xulang Zhang[1], Bo Yu[1,2], Xinmei Wang[1], Yun Wu[1], Lei Li[1], Keliang Gao[1], Xin Hu[1], Xi Zhao[1,2], O. Hemminger[1,2], Wu Lu[1,5], Gregory P. Lafyatis[1,3] and L. James Lee[1,2]*

Many transfection techniques can deliver biomolecules into cells, but the dose cannot be controlled precisely. Delivering well-defined amounts of materials into cells is important for various biological studies and therapeutic applications. Here, we show that nanochannel electroporation can deliver precise amounts of a variety of transfection agents into living cells. The device consists of two microchannels connected by a nanochannel. The cell to be transfected is positioned in one microchannel using optical tweezers, and the transfection agent is located in the second microchannel. Delivering a voltage pulse between the microchannels produces an intense electric field over a very small area on the cell membrane, allowing a precise amount of transfection agent to be electrophoretically driven through the nanochannel, the cell membrane and into the cell cytoplasm, without affecting cell viability. Dose control is achieved by adjusting the duration and number of pulses. The nanochannel electroporation device is expected to have high-throughput delivery applications.

A variety of cell transfection techniques have been developed, including viral vectors[1,2], chemical methods[3] (for example, complexes with lipids, calcium phosphate, polycations or basic proteins) and physical methods (such as particle bombardment, micro-injection and electroporation)[4,5]. Except for micro-injection[6,7], these techniques are based on bulk stochastic processes in which cells are transfected randomly by a large number of genes ($>1 \times 10^8$ per cell)[8]. A disadvantage of such methods is that the injected dose cannot be controlled.

Bulk electroporation (BEP) is the most widely used physical method for transfecting cells because of its technical simplicity, fast delivery and almost no limitation on cell type and size[9–13]. Recently, microfluidics-based electroporation (MEP) has emerged as a new technology that has been developed by a number of researchers[14–20] for individual cell transfection. In MEP, a cell is usually located next to a small aperture (with dimensions of a few micrometres) that focuses the porating electric field to a corresponding area on the cell membrane. MEP offers several important advantages over BEP, including lower poration voltages, better transfection efficiency and a sharp reduction in cell mortality. However, the MEP delivery mechanisms are similar to that in BEP[21–25]—both processes are diffusion dominated and, for large transfection agents such as nucleic acids or quantum dots, entry into the cytosol is effected through an attachment onto the outside of the cell membrane followed by an endocytosis-like process. Precise dose control has not been demonstrated using either BEP or MEP. In contrast, nanochannel electroporation (NEP) exposes an extremely small area of a cell membrane positioned adjacent to a nanochannel to very large local electric field strengths. In this Article, we show that in an NEP device, transfection agents are electrophoretically driven directly into the cell cytosol during poration, with negligible diffusion after poration, and precise dose control is achieved with practically no cell mortality.

The NEP system

The basic element of NEP comprises two microchannels connected by a nanochannel (diameter $\approx$ 90 nm in this study) (Fig. 1). The cell to be transfected is positioned in one microchannel to lie against the nanochannel, and the other microchannel is filled with the agent to be delivered. This unique microchannel–nanochannel–microchannel design enables the precise placement of individual cells. One or more voltage pulses lasting milliseconds is delivered between the two microchannels, causing transfection. Dose control is achieved by adjusting the duration and number of pulses. Alternatively, the voltage and/or agent concentration can be changed.

We recently developed a simple and low-cost DNA combing and imprinting (DCI) method that can be used to form a sealed array of laterally ordered nanochannels interconnected to microchannels with controllable sizes and rounded shape over arbitrarily large surface areas[26] (Fig. 1a). In this study, a DNA-in-buffer was 'combed' to produce an array of stretched DNA nanostrands on a microridge-patterned polymer stamp (Fig. 1a). The stamp was then sputter-coated with gold. The gold-coated DNA strands act as templates for the nanochannels, with the nanochannel diameter being determined by the thickness of the gold coating. The stamp was placed face down on a silanized glass substrate and imprinted by a low-viscosity resin. After curing the resin, the stamp was peeled off the slide, leaving behind an array of microchannels connected by gold-coated DNA nanostrands. The slide was soaked in gold etchant and then rinsed with deionized (DI) water, leaving behind embedded nanochannels connecting the microchannels. Fabrication details are given in the Methods. Associated micro- and macroscale inlets/outlets were also formed in the fabrication process. Each of the two rows of microchannels led to a reservoir into which cells and the transfection material were loaded, respectively. An electrode was placed in each reservoir to carry out

[1]Center for Affordable Nanoengineering of Polymeric Biomedical Devices, Ohio State University, Columbus, Ohio 43210, USA, [2]Department of Chemical and Biomolecular Engineering, Ohio State University, Columbus, Ohio 43210, USA, [3]Department of Physics, Ohio State University, Columbus, Ohio 43210, USA, [4]Department of Mechanical and Aerospace Engineering, Ohio State University, Columbus, Ohio 43210, USA, [5]Department of Electrical and Computer Engineering, Ohio State University, Columbus, Ohio 43210, USA. *e-mail: lee.31@osu.edu

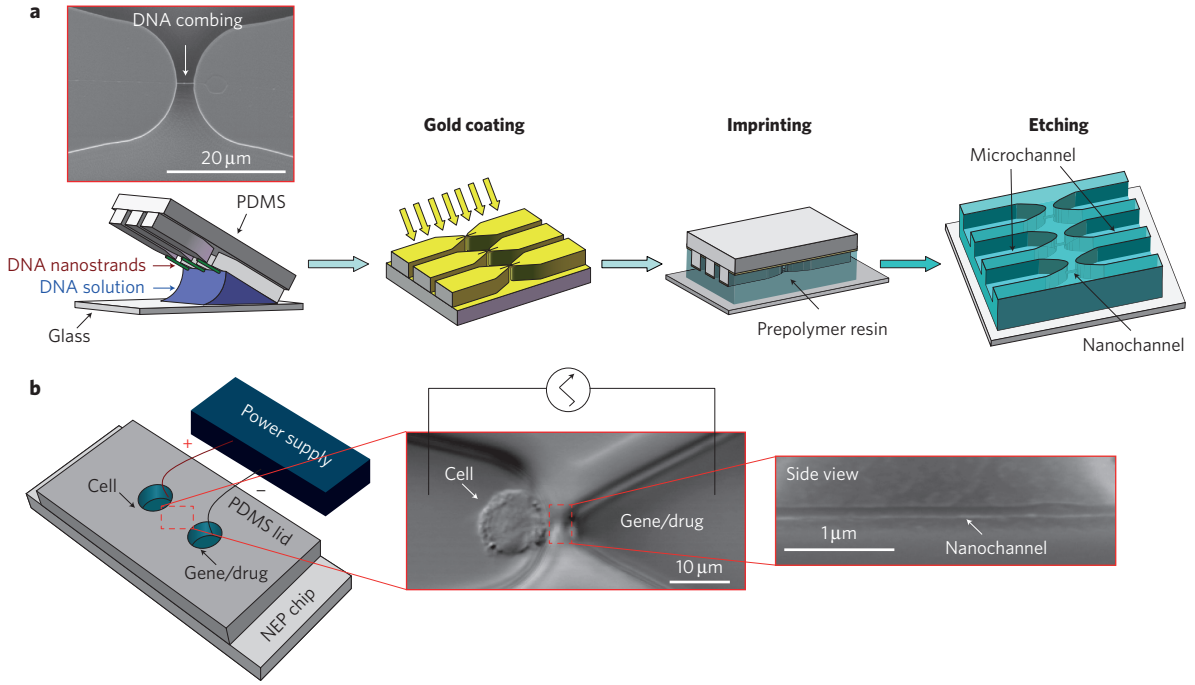

Figure 1 | Apparatus and operation of the NEP device. a, Top: SEM image of a DNA nanostrand (arrow) 'combed' across two PDMS 'microridges'. Bottom: schematic showing the fabrication of the NEP chip by DCI. **b**, Left: schematic of an NEP chip covered by a PDMS lid with electrodes placed in reservoirs. Middle: optical micrograph of a Jurkat cell in the left microchannel and positioned at the tip of the nanochannel using optical tweezers. The right microchannel contains gene or drugs. Right: SEM image of side view cut of a nanochannel. The nanochannel is ~90 nm in diameter and ~3 μm long.

transfection, with voltage pulses varying between 150 and 350 V, depending on the need (Fig. 1b).

An optical tweezers system was connected to our NEP construct. This was used to manipulate a selected cell inside a microchannel and position the cell at the tip of the nanochannel where it would stick. The optical tweezers was moved off the cell before electroporation.

Figure 2a (left) compares NEP transfection using BEP and MEP of K562 cells using propidium iodide (PI) dye. Poration can be identified by cell uptake of the PI dye and subsequent fluorescent signal. For BEP, a single 10 ms pulse with an electric field strength of 70 V mm^{-1} was used. A gradual increase of PI fluorescence (time, ~150 s) was observed (Supplementary Movie S1, Fig. 2b,c), indicating that diffusion after poration is the dominant mechanism for PI transfer. A similar time evolution was observed for electroporation with an MEP device (Supplementary Movie S2, Fig. 2). In contrast, significant acceleration of dye was observed in NEP during poration (Supplementary Movie S3, Fig. 2b,c). After only 30 ms, a strong fluorescent signal was observed in the middle of the cell. Within 2.3 s, the entire cell turned bright. Theoretical analysis shows that a high velocity is reached by molecules in the nanochannel, allowing them to be delivered into the cell during poration by a localized and focused electric field inducing strong electrophoresis (see the table in Fig. 2a). Such a unique feature allows precise delivery of charged reagents into small cells.

Examples of delivery and dosage control

To show dosage control with NEP, Jurkat cells (diameter ≈ 15 μm) were transfected with an 18-mer oligodeoxynucleotide (ODN, G3139) conjugated with Cy3 to allow fluorescent detection. NEP was carried out using a single 220 V/2 mm pulse of varying durations, and the fluorescence signal from ODN uptake was measured (summarized in Fig. 3a; see also Supplementary Movie S4). The amount of ODN transfected is a monotonic function of pulse duration and is near-linear from 5 to 20 ms. A similar dose versus pulse length dependence was also seen for leukaemia-patient cells as small as 8 μm in diameter (Supplementary Fig. S13). Two tests were carried out to investigate the repeatability of NEP. Five cells were simultaneously transfected in an NEP array. Next, another five cells were individually transfected using identical NEP settings (Fig. 3b). The cell-to-cell variation in the amount of ODN delivered was ±10% and ±12%, respectively.

In a second example, the delivery of a GAPDH molecular beacon (MB) by NEP was investigated. GAPDH–MB is a messenger RNA (mRNA) probe with a fluorophore at one end and a quencher at the other end of a stem–hairpin structure (Fig. 3c)[27,28]. After hybridization with complementary targets, the fluorescence is restored by separating the fluorophore and the quencher, allowing real-time expression and localization of specific mRNA inside the living cells. Figure 3d shows that successful delivery of GAPDH–MB resulted in red fluorescence inside a cell. A mismatch-MB probe (scrambled) was also transferred as negative control to confirm the selectivity of the MB. Figure 3e summarizes the fluorescence intensity inside the cells at different conditions. The plateau of the GAPDH–MB signal with a long enough pulse length or multiple pulses indicates that all GAPDH in the cell has been detected. As NEP quickly delivers probes into the cell, time-dependent fouling of MB is avoided[27].

We next used the dosage control capability of NEP to study the transfection of K562 cancer cells with siRNA(Mcl-1)[29]. The protein Mcl-1 inhibits programmed cell death (apoptosis) and thus promotes the survival of lymphocytes and haematopoietic stem cells[30–32]. It is linked to drug resistance and poor treatment outcomes in many tumour types. SiRNA(Mcl-1) down-regulates Mcl-1 and, at sufficient dosage, can induce the apoptotic death of a target cell. Figure 4 shows NEP experiments that were conducted to determine the critical dosage of siRNA(Mcl-1) for killing K562 cells. For pulses longer than 5 ms at 220 V/2 mm, a fatal dose of siRNA(Mcl-1) was delivered to cells (indicated by the red fluorescence). However, most cells remained viable for pulses shorter than 2 ms

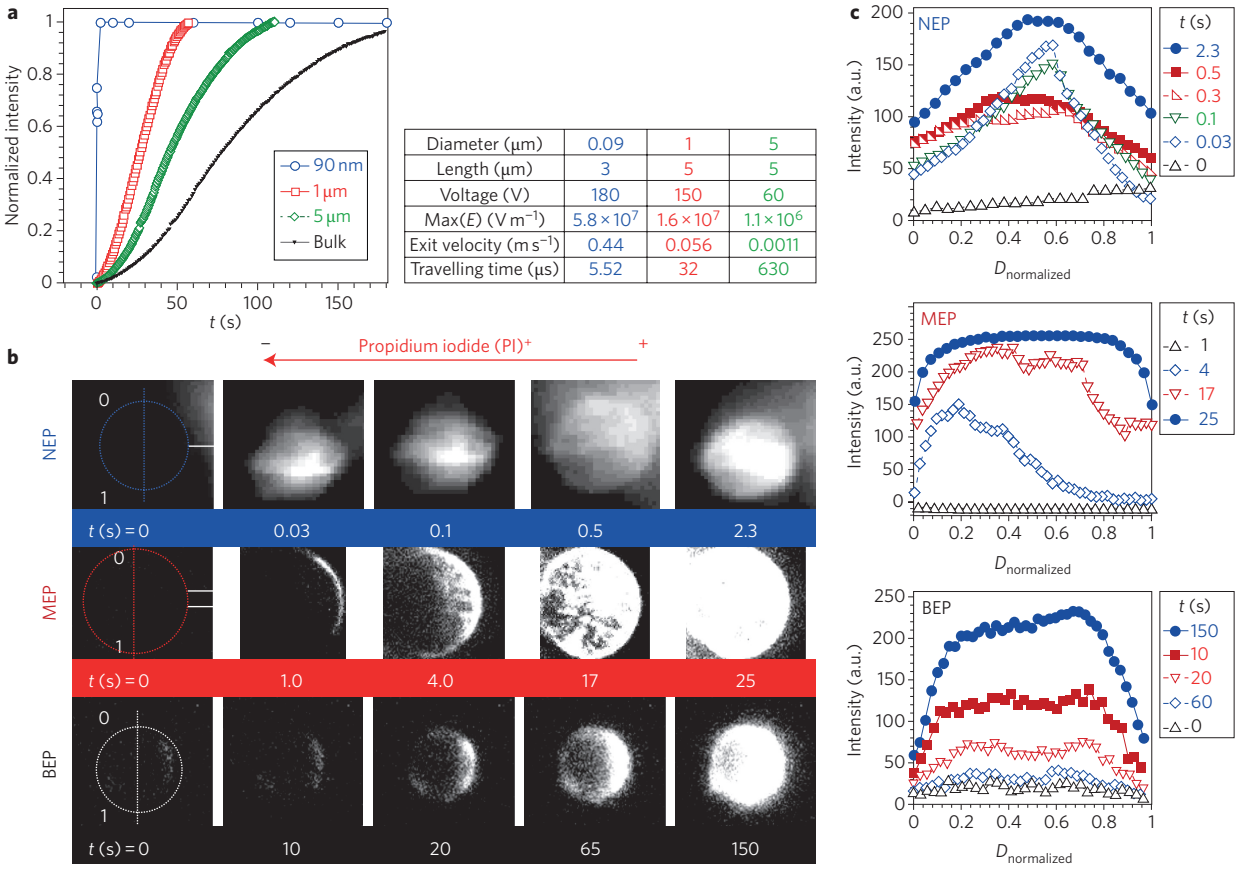

Diameter (μm)	0.09	1	5
Length (μm)	3	5	5
Voltage (V)	180	150	60
Max(E) (V m^{-1})	5.8×10^7	1.6×10^7	1.1×10^6
Exit velocity (m s^{-1})	0.44	0.056	0.0011
Travelling time (μs)	5.52	32	630

Figure 2 | Comparison of NEP with BEP and MEP. a, Left: time dependence of PI dye uptake for NEP (180 V/2 mm, blue curve), BEP (70 V/mm, black) and MEP (150 V/2 mm for 1 μm (red) and 60 V/2 mm for 5 μm (green) cases). All used a single 10 ms pulse. Right: results of the finite-element simulation for the channel, including the maximum electric field (max(E)), the electrophoretic exit velocity and the channel transit time (assuming an electrophoretic mobility of 1×10^{-8} m^2 V^{-1} s^{-1} for the PI dye). **b**, Fluorescence micrographs of a cell after being transfected with PI dye by NEP, MEP (1 μm case) and BEP. Conditions are as in **a**. The time series of captured images is specified at the bottom of each image. Solid white horizontal lines show the location of micro/nanochannels. The loaded cells in NEP, MEP and BEP devices are specified by dotted circles. The transverse axis was defined by dotted lines to measure the intensity across the cell section (0–1 represents the distance from top to bottom of the cell). **c**, Fluorescence intensity profile along the transverse axis of the cell (shown in **b**) at different times.

(green fluorescence). Statistical variations of the critical dosage for individual cells were studied using NEP with pulse lengths from 2 to 10 ms; between 7 and 11 cells were used for each pulse length. Figure 4 summarizes the cell viability measurements. Fluorescence photographs are provided in Supplementary Fig. S18. A parallel set of transfections using the same pulsing parameters but a scrambled siRNA is shown in the 'control' columns. None of these resulted in cell death.

Theoretical analysis of NEP

We next describe our current theoretical understanding of NEP. Our analysis is based on the following four key features. First, all important activity for the process takes place in or near the nanochannel. Electrically, the microchannels in our microchannel–nanochannel–microchannel set-up are simply high-conductance 'wires' to the nanochannel. Second, except for initial nanosecond transients, almost all the voltage drop is across the extremely high-resistance nanochannel ($R_{NC} \approx 600$ MΩ). Electrically, this is a classical 'current source', $i_{NC} = V_{applied}/R_{NC}$, and plays a controlling role in the NEP process. It makes transfection repeatable by minimizing sensitivity to process details, for example, electrode placement or small voltage drops across various membranes. The third key feature describes the actual transfection mechanism. Charged transfection molecules are rapidly (<10 μs) swept by electrophoresis through the nanochannel and end up in the cell. Residual fields in the cell itself can further distribute the transfecting agent. Finally, significant transfection occurs only during the applied voltage pulse, during which delivery of the agent is intense and highly localized. In contrast to other electroporation methods, the diffusion of transfection molecules through residual pores after the voltage pulse has terminated is negligible.

Figure 5a (left) shows the physical layout for NEP. Supplementary Section 2A contains an extended version of the circuit model presented here and detailed analysis based on finite-element simulations. We assume that cell–nanochannel sealing is perfect (effects of cell placement are discussed in Supplementary Section 2B). Figure 5a (right) is an equivalent circuit for a model system with a 90-nm-diameter, 3-μm-long nanochannel before electroporation. Equivalent resistances and capacitances in the model are calculated for a 15 μm cell using accepted values for the conductivities and permeabilities of the buffer solution and the cell membrane (Supplementary Table S1). The equivalent resistances of the microchannels are negligible (<1 MΩ), and the cell interior is well modelled as a perfect conductor. The cell membrane is divided into two parts (Fig. 5a). Membrane 1 refers to the section adjacent to the nanochannel and membrane 2 to the remainder. A real cell membrane is a complex construct of lipids with embedded proteins, including conducting channels and transporters.

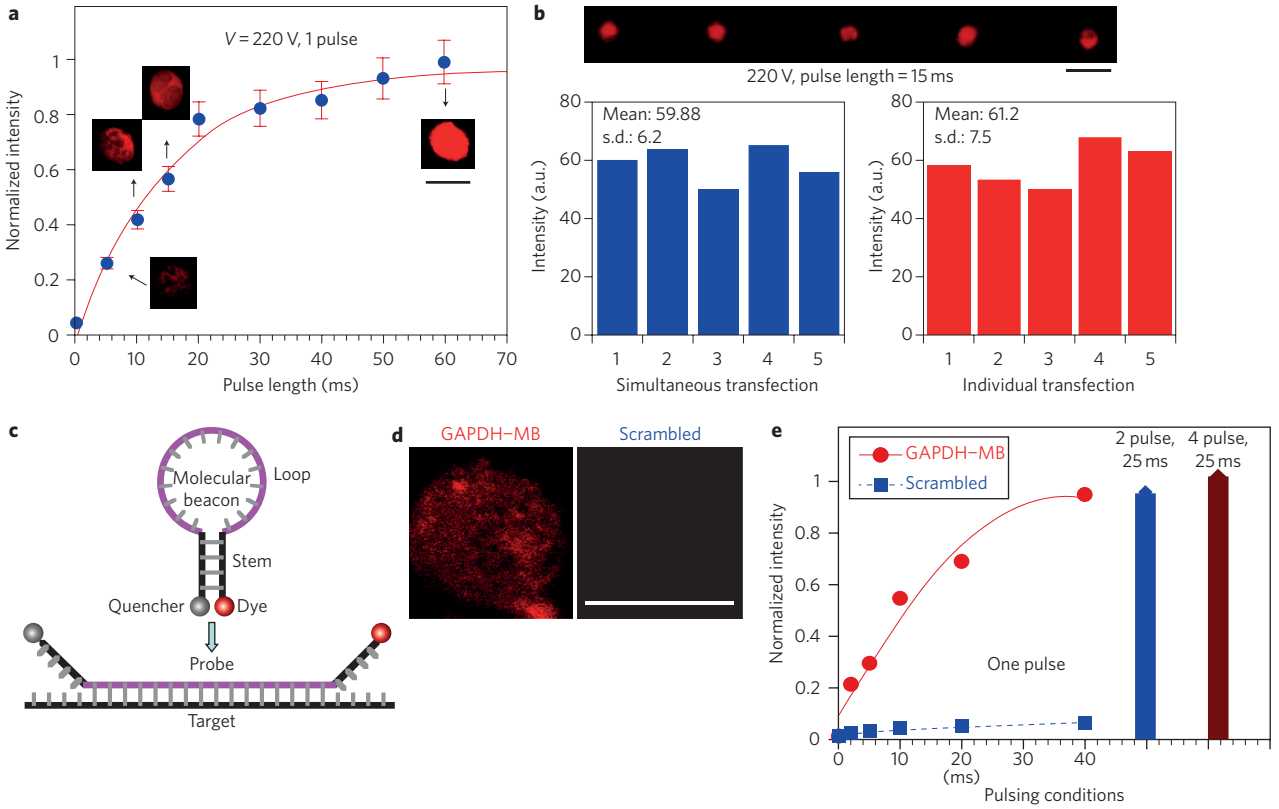

Figure 3 | Dosage control by NEP. a, Jurkat cells transfected with Cy3-ODN using single 220 V/2 mm pulses of varying durations. Transfection is quantified by the fluorescence signals, which are normalized to the intensity at 60 ms (scale bar, 15 μm). The saturating fluorescence fits a saturating exponential function. **b**, Top: fluorescence micrographs of five cells transfected by NEP chip (scale bar, 60 μm). Bottom: five cells are transfected simultaneously (left) and individually (right) by NEP, showing the repeatability and reliability of the NEP performance. Intensity is expressed in arbitrary units (a.u.). s.d., standard deviation. **c**, Molecular beacon (MB) before hybridization shows dye is quenched (top). After hybridization with target, fluorescence is restored (bottom). **d**, A Jurkat cell transfected (220 V/2 mm) with GAPDH-MB produced fluorescence, but a cell transfected with a scrambled sequence remained dark (scale bar, 15 μm). **e**, Relative MB fluorescence intensities for various pulsing programmes (measured 45 min after NEP).

Following previous electroporation modellers[33–35], we treat an electrically intact cell membrane as a resistance in parallel with a capacitance. Values in the literature for cell membrane conductivity vary by two orders. The applied voltage satisfies $V_{applied} = V_{NC} + V_{TM1} + V_{TM2}$. We assume that when the voltage across a membrane exceeds some small value (~1 V), that membrane porates.

The NEP process is readily described. On application of a voltage pulse, the potential across membrane 1 (facing the nanochannel) rapidly increases. This membrane reaches the critical voltage in nanoseconds and porates. Assuming that the now-porated membrane 1 presents a negligible resistance, the second 'outer' membrane starts charging and within tens of microseconds, a steady-state current is reached. Two observations can be based on this model. First, for 99% of the pulse, the cell has a steady-state, nanochannel-limited current ($i_{NC} = V_{applied}/R_{NC}$) flowing through it. Assuming the transfection agent makes up a constant fraction of this current, this explains the near-linear relationship between pulse length and dose. Second, depending on the model details, membrane 2 may charge to an unsustainable voltage and porate. Although we usually observe no dye movement across that membrane, current may be carried by small ions. Such putative pores could challenge cell viability when transfecting sensitive cells.

During the pulse, almost the entire applied voltage appears across the nanochannel, and the generated electric fields are enormous (70 MV m^{-1} for a 200 V pulse). This produces large electrophoretically driven drift velocities; 700 μm ms^{-1} is typical for quantum dots. Transfection therefore occurs as follows. Charged transfection agents enter the nanochannel through a combination of drift and diffusion and, within a few microseconds, are swept into the cell. In our finite-element simulations, we find that fringe fields extend into the cell and can 'inject' agents through the cell membrane and into the cytoplasm (Fig. 5b).

We note that the pore creation mechanism in NEP may be different from that of BEP and MEP. Experimentally, a striking feature is that large transfection agents, such as DNA and quantum dots, appear almost instantly inside the cytoplasm with NEP, but are not observed when using other types of electroporation. This suggests that large pores are created in the cell membrane adjacent to the nanochannel during the electrical pulse.

NEP versus MEP and BEP

As noted in Fig. 2b, dye uptake occurs differently for BEP and MEP than for NEP. For both BEP and MEP, uptake is predominantly a diffusion-dominated process that occurs largely subsequent to electrical pulsing[11,36]. In contrast, in NEP, a sharp peak of the fluorescent intensity is observed in the middle of the cell at $t = 0.03$ s, that is, simultaneously with the electrical pulse, and no further PI dye diffusion into the cell is observed after poration. This observation is consistent with the theory that a highly localized and focused electric field and strong electrophoresis at the nanoscale induce strong convective injection, resulting in fast uptake of the PI dye during poration.

There is a need to inject cells with nanoprobes, such as quantum dots. Their bright and stable fluorescence and/or manipulability, as well as their small size, make them suited to revealing biological mechanisms and processes at an unprecedented level of detail.

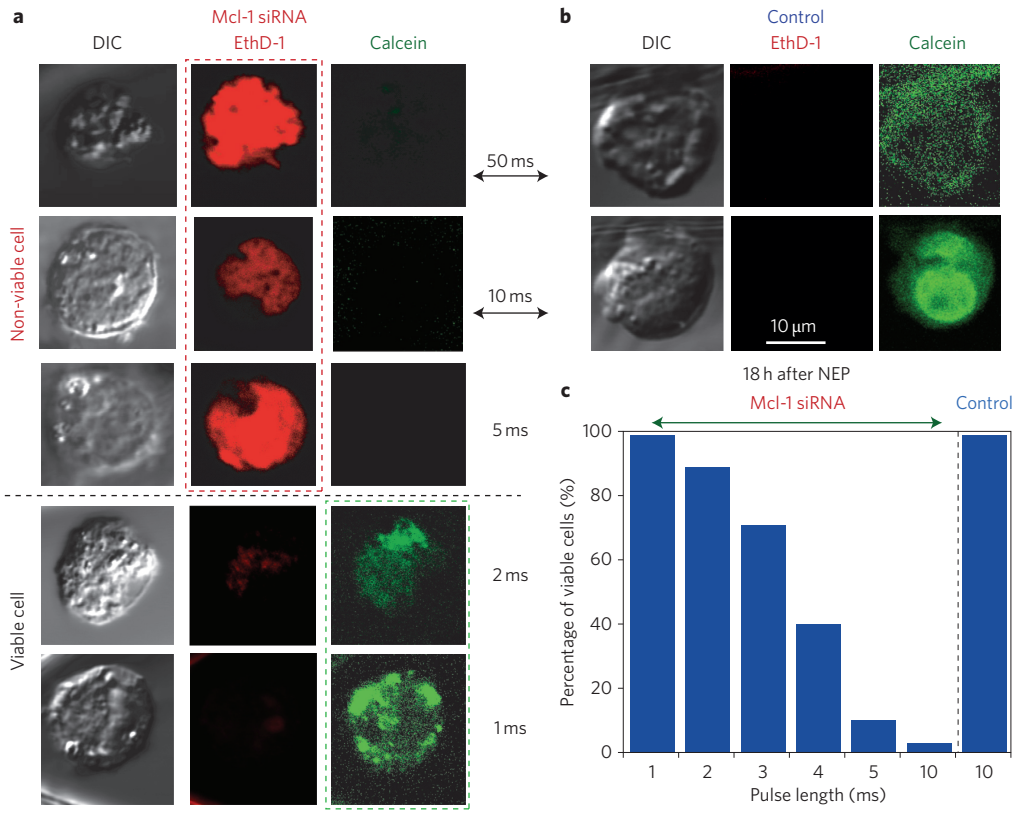

Figure 4 | Critical siRNA dosage to kill cancer cells by NEP. Viability of K562 cancer cells was measured using the LIVE/DEAD assay 18 h after transfection with Mcl-1 siRNA, which downregulates the Mcl-1 protein that inhibits apoptosis. Calcein AM produces green fluorescence in live cells (excitation, 488 nm; emission, 507 nm), and ethidium homodimer (EthD-1) enters cells with damaged membranes and produces red fluorescence in dead cells (excitation, 530 nm; emission, 595 nm). **a**, For NEP pulse durations of 5 ms or longer, sufficient amounts of siRNA entered the cells and the Mcl-1 protein was sufficiently downregulated to induce apoptosis (red dashed box); cells pulsed for 5 ms or less did not receive sufficient amounts of siRNA and therefore remained viable (green dashed box). **b**, All control cells transfected with scrambled siRNA sequence remained alive. **c**, Cell viability under different pulse durations of siRNA (Mcl-1) injection at 220 V/2 mm (pulse length = 1, 2, 3, 4, 5 and 10 ms; number of cells = 8, 9, 7, 7, 8 and 7, respectively).

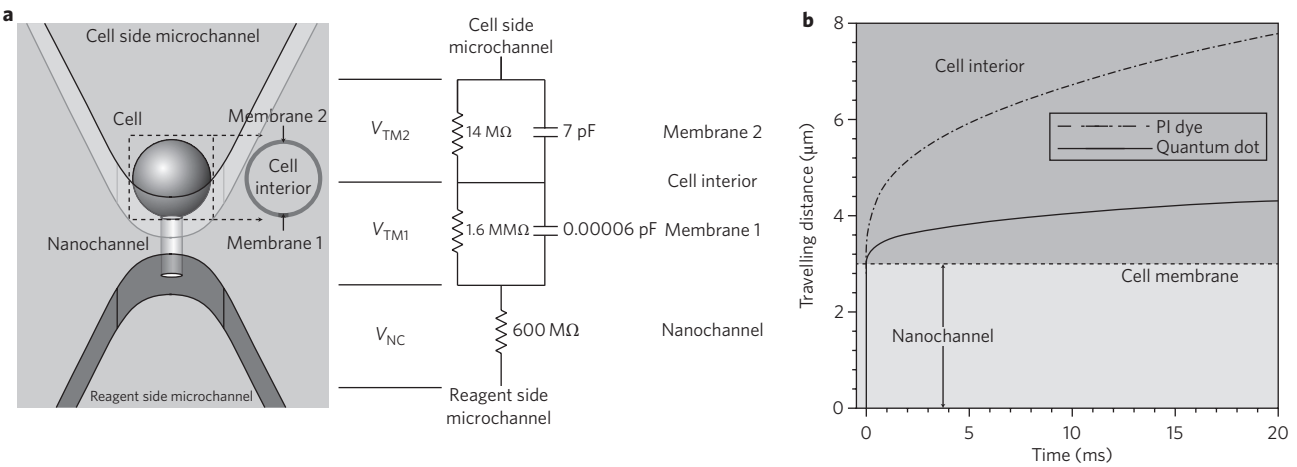

Figure 5 | Theoretical analysis of NEP. a, Left: schematic of cell in an NEP device. Right: equivalent electrical circuit of the electroporation system for an intact cell in NEP. **b**, Transport of transfection agents into a cell. The zero of the vertical axis is the entrance of the nanochannel. During the pulse, fringe fields extending into the cell drive molecules through the cell membrane and deep into the cytosol.

Additionally, the ability to deliver controlled numbers of quantum dots or other nanoparticles to the cell cytoplasm provides a unique opportunity for quantitative studies of cytotoxicity of nanoparticles such as carbon nanotubes and gold, silver and metal oxide particles. Ideally, nanoprobes would be delivered uniformly to all parts of the cell. Existing delivery techniques have difficulty in achieving any significant transfection of these relatively large-sized probes without causing unintended side effects. Most such methods rely on a non-specific endocytosis process and have the disadvantage that internalized quantum dots are often trapped within endosomal compartments, which may block their ability to reach specific intracellular targets[37].

We carried out a study comparing the abilities of BEP, MEP and NEP to transfect Jurkat cells with quantum dots conjugated with a

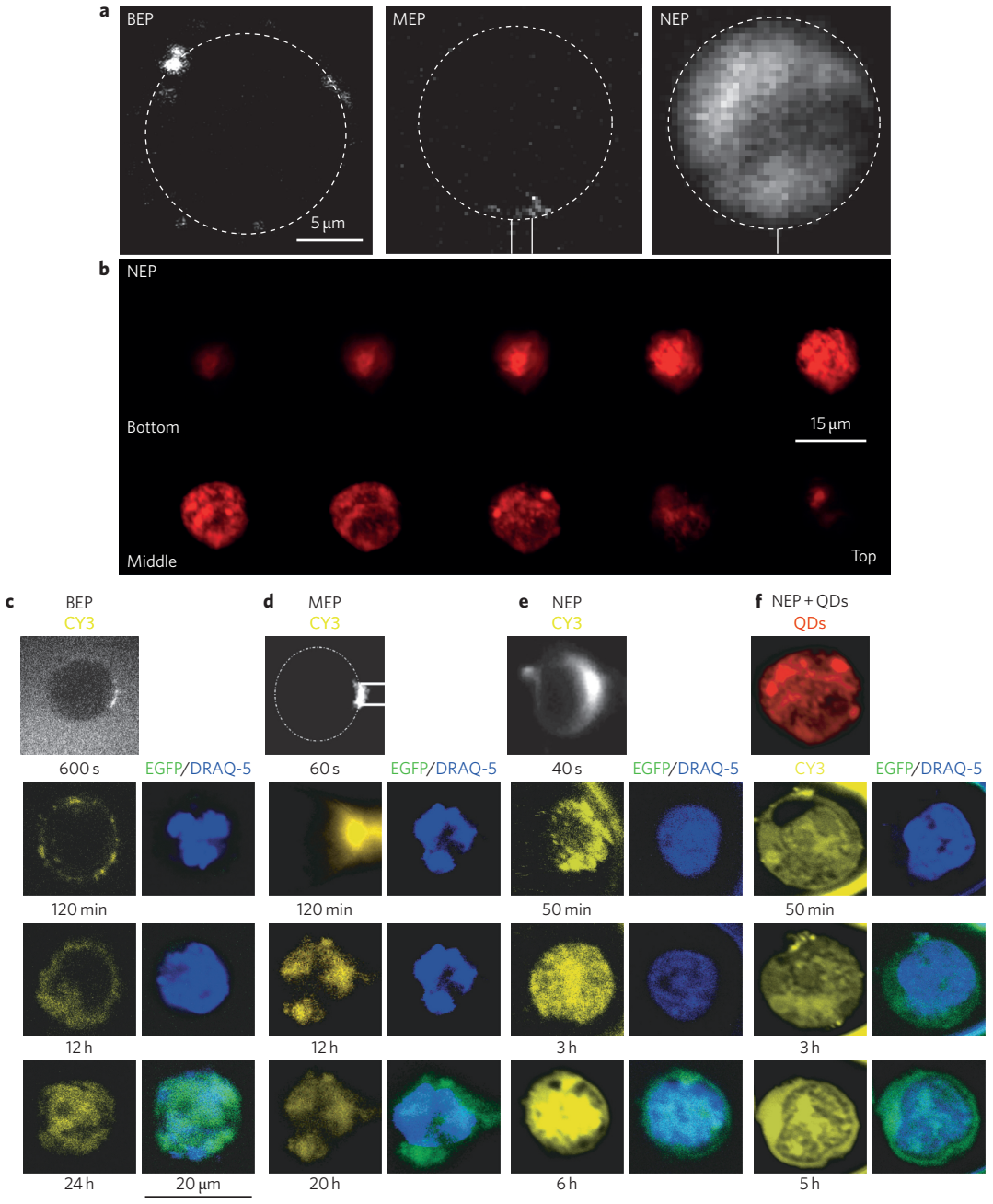

Figure 6 | Delivery of nanoparticles and plasmids to Jurkat cells. a, Quantum dots delivered by BEP, MEP (1 μm) and NEP at 600, 60 and 14 s, respectively, after poration. Location of micro/nanochannels is specified by solid white vertical lines. **b**, Z-stack of confocal microscope images (step size, 1.1 μm) of a cell NEP-porated with 3.5 kbp Cy3-labelled GFP plasmid in a single cell, with the top left image representing the bottom of the cell and the bottom right image the top of the cell. **c**–**f**, Comparison of the delivery of GFP plasmid by BEP (**c**), MEP (5 μm) (60 V/2 mm, two 10 ms pulses) (**d**), NEP (260 V/2 mm, two 5 ms pulses) (**e**) and NEP + quantum dots (QDs) after poration (**f**). Fluorescence images: Cy3 (yellow), nucleus (DRAQ-5, blue) and GFP fluorescence (green). BEP was carried out on a NEON transfection system at 1,325 V with three 10 ms pulses for ~1×10^5 cells. See Supplementary Fig. S14 for transfection of pCAG-GFP plasmid (~6.6 kbp) into mouse embryonic fibroblast cells.

Table 1 | Biomolecule and quantum dot data.

Sample	Concentration (nM)	Zeta potential (mV)	Size
COOH-QD	10	−17 ± 2.13	$r = 10$ nm
ODN-Cy3	50	−10.09 ± 3.76	18 mer ≈ 6,000 g mol^{-1}
Mcl1-siRNA	50	−10.15 ± 4.35	21 nt ≈ 14,000 g mol^{-1}
MB-Cy3	50	−11.01 ± 5.35	34 mer ≈ 10,000 g mol^{-1}
GFP-pMAX	50	−15.01 ± 6.4	3.5 kbp ≈ 2.2×10^6 g mol^{-1}
GFP-pCAG	50	−20 ± 3.5	6.6 kbp ≈ 4.2×10^6 g mol^{-1}

COOH group ($r = 10$ nm) (Fig. 6a). Neither BEP nor MEP could deliver these nanoparticles directly into cells; all the quantum dots remained stuck at the cell membrane, where perhaps later some might enter the cell via endocytosis. However, our NEP platform readily internalized the quantum dots inside the Jurkat cells. A uniform spatial distribution of quantum dots inside a transfected cell 30 min after poration is shown in Fig. 6b. A broad spray of quantum dots occurred in the cytoplasm only 14 s after poration (Fig. 6a, right). Other biomolecules such as DNA, RNA and molecular probes can be conjugated onto quantum dots and delivered into cells

in a similar way[38–40]. Supplementary Fig. S10 shows that a small number of quantum dots can also be controllably delivered by NEP.

To study NEP for larger transfection agents, a Cy3-labelled GFP plasmid (3.5 kbp) was used to visualize the gene transfection process of Jurkat cells. Again, we compare NEP with conventional BEP and MEP. In BEP and MEP, DNA 'complexes' formed on the outside of the cell followed by an endocytosis-like passage into the cytoplasm that required more than an hour for BEP (Fig. 6c; Supplementary Fig. S14) and >60 s for MEP (Fig. 6d). This is similar to previously reported observations[11]. Migration to the nucleus and subsequent transcription required many hours. GFP fluorescence was not observed even 18 h after transfection. On the other hand, NEP injects the plasmid directly into the cytoplasm: within 40 s of poration, a significant Cy3 fluorescence was observed inside the cell membrane. Migration of the DNA to the nucleus and transcription occurred in 6 h (Fig. 6e). For higher gene transfection, nanoparticles such as gold or quantum dots can be used to facilitate delivery, roughly analogous to the role of the needle in micro-injection. Figure 6f shows the NEP transfection of a Jurkat cell using a mixture of quantum dots with the (not attached) GFP plasmid. This procedure led to strong GFP expression within 3 h. A viability/cytotoxicity assay confirmed the transfected cells shown in Fig. 6 to be alive.

Conclusions

We have shown that NEP (designed to have a nanochannel between two microchannels) is able to deliver precise amounts of transfection agents into cells without harming the cells. Cells are precisely placed in one microchannel of the device each time with optical tweezers, and transfection occurs when an electrical pulse is delivered between the two microchannels. The extremely large electric fields in the nanochannel electrophoretically accelerate transfection molecules into the cell. After the pulse, any additional, diffusively driven transfection is limited by the small conductance of the nanochannel. Whereas BEP and MEP create large numbers of small pores over a significant fraction of a cell surface, NEP appears to create either a single very large pore or several large pores in the cell membrane adjacent to the nanochannel. In NEP, because the affected area of the cell membrane is very limited (less than 1% of even a small-area MEP device), none of our experiments resulted in cell death. The large NEP pore(s) allowed efficient transfection of relatively large agents directly into the cell cytosol, thus avoiding the endocytosis-to-endosome route on which other electroporation methods rely.

In the future, both experimental work and improved modelling will be needed to better characterize the NEP process. Absolute quantitative calibration of dosage may be accomplished by comparing fluorescence measurements with single-cell polymerase chain reaction. Because some applications require large cell samples, robotic controls can be implemented to allow simultaneous transfection of hundreds of cells. We are presently developing a mechanical loading system that would allow the transfection of 100,000 cells (Supplementary Figs S15–S17).

Methods

NEP fabrication and operation. The DCI process[26] is schematically shown in Fig. 1a. In brief, 0.5 wt% calf thymus DNA (75 kbp, USB Co.) in TE buffer was prepared to produce an array of stretched DNA nanostrands on the microridge-patterned PDMS stamp. The stamp was then sputter-coated with gold (Emitech K550X, Energy Beam Science Inc.) and placed face down on a silanized glass substrate with 3-trimethoxysilylpropyl methacrylate (Sigma-Aldrich). An ethylene glycol dimethacrylate (EGDMA) (Sigma-Aldrich) resin (93 wt% EGDMA, 6 wt% hydroxyethyl methacrylate (HEMA) and 1 wt% Irgacure 651 initiator) was used as an imprinting resin and cured using ultraviolet light (wavelength, 365 nm; intensity, 4 mW cm^{-2}) for 20 min under nitrogen. The stamp was then peeled off the slide, leaving behind the array of PEGDMA microchannels connected by gold-coated DNA nanostrands. To remove gold-coated DNA nanostrands, the slide was soaked in gold etchant (GE8111, Transene Company Inc.) for 48 h and then thoroughly rinsed with DI water, leaving behind embedded nanochannels connecting the microchannels. The chip was soaked in Piranha solution (H_2SO_4/H_2O_2, 7:3) for 3 h to make it hydrophilic. The chip was rinsed with DI water three times and soaked in 0.1% bovine serum albumin (BSA) containing DI water for 30 min to reduce the adhesion between the loaded cells and the substrate.

In single-cell BEP/MEP/NEP experiments, cells ($\sim 1 \times 10^5$ cells per ml) in suspension were centrifuged for 5 min at 5,000 r.p.m. to remove the culture medium and re-suspended in phosphate buffered saline (PBS) media for 5–10 min before poration. Cells were manipulated using optical tweezers built from a 3 W, 1,064 nm laser (Crystal Laser) and an inverted microscope (Olympus IX-71 and Nikon Eclipse TE2000). Typically, 600 mW of power was used to manoeuvre and load a cell close to the tip of the nanochannel. An electron-multiplying charge-coupled device camera (Photometrics Cascade II: 512 EMCCD) was used to detect the fluorescence emission. An electronic pulser from a Bio-RAD Gene Pulser Xcell electroporation system was used to provide the required voltage pulse sequences. Palladium wires (diameter = 0.25 mm, Invitrogen/Molecular Probes) were used as electrodes and were connected to the electronic pulser. MEP fabrication and operation are described in the Supplementary Information. The single-cell BEP experiment is described in a previous publication[36].

Cell culture. Jurkat cells (human T-cell lymphoblast-like cell line) and K562 human erythroleukaemia cells were obtained from the American Type Culture Collection (ATCC). Mouse embryonic fibroblasts were derived from 129/SV-E mice (Charles River Laboratories International). Chronic lymphocytic leukaemia (CLL) patient cells were provided by J. Byrd's laboratory in the Comprehensive Cancer Center at The Ohio State University. Cells were routinely cultured in 25 T flasks containing 5 ml of RPMI-1640 culture medium (Invitrogen) supplemented with 10% fetal bovine serum (FBS, Invitrogen 16000), 100 U ml^{-1} penicillin/100 μg ml^{-1} streptomycin (Invitrogen). Cells were seeded into T flasks at a concentration of 3×10^5 viable cells per ml, incubated at 37 °C in a humidified atmosphere containing 5% CO_2, and subcultured every two days.

Computational modelling of transmembrane potential and electrophoresis. The contact resistance method and the finite-element commercial software COMSOL (Mathworks Inc.) with MATLAB was used to calculate the transmembrane potential[15], electric field distribution and electrophoretic velocity of molecules inside the nano/microchannels. Details are given in the Supplementary Information.

Biomolecule construction. Cy3-modified phosphorothioate oligos G3139 (Cy3-G3139) (sequence: 5′-TCT CCC AGC GTG CGC CAT-3′) was custom synthesized by Alpha DNA. The molecular beacon against GAPDH (GAPDH–MB: 5′-Cy3-CGA CGG AGT CCT TCC ACG ATA CCA CGT CG-BHQ2a-Q-3′) and the control molecular beacon (Control–MB: 5′-Cy3-GCG AGG GTA GAT GCA GCC TTG TCT ATA CCC TCG C-BHQ2a-Q-3′) were purchased from Eurofins MWG Operon. The Mcl-1 specific siRNA was purchased from Ambion (sense: 5′-GGUCCAUGUUUUCAAAGAUtt-3′; anti-sense: 5′-AUCUUUGAAAACAUGGACCat-3′). pMax-GFP (3.5 kbp, 0.5 μg μl^{-1}) and pCAG-GFP (6.6 kbp, 0.5 μg μl^{-1}) were purchased from Amaxa Biosystems and Addgene, respectively. The GFP plasmids were labelled with CY3 dye using Label IT CyTM3 Labeling kit (Mirus). 585-655 ITK carboxyl quantum dots solution was purchased from Invitrogen.

Zeta potential and size. The zeta potential of biomolecules was determined using a PALS zeta potential analyser (Brookhaven Instrument Corp). This information and other characteristics of biomolecules and quantum dots are listed in Table 1.

Received 3 May 2011; accepted 5 September 2011; published online 16 October 2011

References

1. Nayak, S. & Herzog, R. W. Progress and prospects: immune responses to viral vectors. *Gene Ther.* **17,** 295–304 (2010).
2. Wu, S. C., Huang, G. Y. L. & Liu, J. H. Production of retrovirus and adenovirus vectors for gene therapy: a comparative study using microcarrier and stationary cell culture. *Biotechnol. Progr.* **18,** 617–622 (2002).
3. Schmid, R. M. *et al.* Liposome mediated gene transfer into the rat oesophagus. *Gut* **41,** 549–556 (1997).
4. O'Brien, J. A. & Lummis, S. C. R. Biolistic transfection of neuronal cultures using a hand-held gene gun. *Nature Protoc.* **1,** 977–981 (2006).
5. Wells, D. J. Gene therapy progress and prospects: electroporation and other physical methods. *Gene Ther.* **11,** 1363–1369 (2004).
6. Capecchi, M. R. High efficiency transformation by direct microinjection of DNA into cultured mammalian cells. *Cell* **22,** 479–488 (1980).
7. Nagy, A., Gertsenstein, M., Vintersten, K. & Behringer, R. *Manipulating the Mouse Embryo: A Laboratory Manual* (Cold Spring Laboratory, 2003).
8. Luo, D. & Saltzman, W. M. Synthetic DNA delivery systems. *Nature Biotechnol.* **18,** 33–37 (2000).
9. Zimmermann, U. & Neil, G. A. *Electromanipulation of Cells* (CRC Press, 1995).

10. Coulberson, A. L., Hud, N. V., LeDoux, J. M. & Vilfan, I. D. Gene packaging with lipids, peptides and viruses inhibits transfection by electroporation *in vitro*. *J. Control. Rel.* **86,** 361–370 (2003).
11. Golzio, M., Teissie, J. & Rols, M. P. Direct visualization at the single-cell level of electrically mediated gene delivery. *Proc. Natl Acad. Sci. USA* **99,** 1292–1297 (2002).
12. Prasanna, G. L. & Panda, T. Electroporation: basic principles, practical considerations and applications in molecular biology. *Bioproc. Eng.* **16,** 261–264 (1997).
13. Costa, M. *et al.* A method for genetic modification of human embryonic stem cells using electroporation. *Nature Protoc.* **2,** 792–796 (2007).
14. Kurosawa, O. *et al.* Electroporation through a micro-fabricated orifice and its application to the measurement of cell response to external stimuli. *Meas. Sci. Technol.* **17,** 3127–3133 (2006).
15. Fei, Z. *et al.* Micronozzle array enhanced sandwich electroporation of embryonic stem cells. *Anal. Chem.* **82,** 353–358 (2010).
16. Fox, M. B. *et al.* Electroporation of cells in microfluidic devices: a review. *Anal. Bioanal. Chem.* **385,** 474–485 (2006).
17. Wang, M., Orwar, O. & Weber, S. G. Single-cell transfection by electroporation using an electrolyte/plasmid-filled capillary. *Anal. Chem.* **81,** 4060–4067 (2009).
18. Wang, S., Zhang, X., Wang, W. & Lee, L. J. Semicontinuous flow electroporation chip for high-throughput transfection on mammalian cells. *Anal. Chem.* **81,** 4414–4421 (2009).
19. Huang, Y. P. & Rubinsky, B. Micro-electroporation: improving the efficiency and understanding of electrical permeabilization of cells. *Biomed. Microdev.* **2,** 145–150 (1999).
20. Khine, M., Lau, A., Ionescu-Zanetti, C., Seo, J. & Lee, L. P. A single cell electroporation chip. *Lab Chip* **5,** 38–43 (2005).
21. Golzio, M. *et al.* Control by osmotic pressure of voltage-induced permeabilization and gene transfer in mammalian cells. *Biophys. J.* **74,** 3015–3022 (1998).
22. Klenchin, V. A., Sukharev, S. I., Serov, S. M., Chernomordik, L. V. & Chizmadzhev, Y. A. Electrically induced DNA uptake by cells is a fast process involving DNA electrophoresis. *Biophys. J.* **60,** 804–811 (1991).
23. Sukharev, S. I., Klenchin, V. A., Serov, S. M., Chernomordik, L. V. & Chizmadzhev, Y. A. Electroporation and electrophoretic DNA transfer into cells. The effect of DNA interaction with electropores. *Biophys. J.* **63,** 1320–1327 (1992).
24. Glaser, R. W., Leikin, S. L., Chernomordik, L. V., Pastushenko, V. L. & Sokirko, A. I. Reversible electrical breakdown of lipid bilayers: formation and evolution of pores. *Biochim. Biophys. Acta* **940,** 275–287 (1988).
25. Mir, L. M. *et al.* High-efficiency gene transfer into skeletal muscle mediated by electric pulses. *Proc. Natl Acad. Sci. USA* **96,** 4262–4267 (1999).
26. Guan, J. *et al.* Large laterally ordered nanochannel arrays from DNA combing and imprinting. *Adv. Mater.* **22,** 3997–4001 (2010).
27. Santangelo, P., Nitin, N. & Bao, G. Nanostructured probes for RNA detection in living cells. *Ann. Biomed. Eng.* **34,** 39–50 (2006).
28. Sokol, D. L., Zhang, X. L., Lu, P. Z. & Gewitz, A. M. Real time detection of DNA RNA hybridization in living cells. *Proc. Natl Acad. Sci. USA* **95,** 11538–11543 (1998).
29. Aichberger, K. J. *et al.* Identification of mcl-1 as a BCR/ABL-dependent target in chronic myeloid leukemia (CML): evidence for cooperative antileukemic effects of imatinib and mcl-1 antisense oligonucleotides. *Blood* **105,** 3303–3311 (2005).
30. Dzhagalov, I., St. John, A. & He, Y. The antiapoptotic protein Mcl-1 is essential for the survival of neutrophils but not macrophages. *Blood* **109,** 1620–1626 (2007).
31. Pellegrini, M. & Strasser, A. A portrait of the Bcl-2 protein family: life, death, and the whole picture. *J. Clin. Immunol.* **19,** 365–377 (1999).
32. Youle, R. J. & Strasser, A. The BCL-2 protein family: opposing activities that mediate cell death. *Nature Rev. Mol. Cell Biol.* **9,** 47–59 (2008).
33. Gowrishankar, T. R. & Weaver, J. C. An approach to electrical modeling of single and multiple cells. *Proc. Natl Acad. Sci. USA* **100,** 3203–3208 (2003).
34. Krassowska, W. & Filev, P. D. Modeling electroporation in a single cell. *Biophys. J.* **92,** 404–417 (2007).
35. Kotnik, T., Bobanovic, F. & Miklavcic, D. Sensitivity of transmembrane voltage induced by applied electric fields—a theoretical analysis. *Bioelectrochem. Bioenerg.* **43,** 285–291 (1997).
36. Henselee, B., Morss, A., Hu, X., Lafyatis, G. P. & Lee, L. J. Electroporation dependence on cell size: an optical tweezers study. *Anal. Chem.* **83,** 3998–4003 (2011).
37. Delehanty, J. B., Mattoussi, H. & Medintz, I. L. Delivering quantum dots into cells: strategies, progress and remaining issues. *Anal. Bioanal. Chem.* **393,** 1091–1105 (2009).
38. Chen, X., Kis, A., Zettl, A. & Bertozzi, C. R. A cell nanoinjector based on carbon nanotubes. *Proc. Natl Acad. Sci. USA* **104,** 8218–8222 (2007).
39. Yum, K., Na, S., Xiang, Y., Wang, N. & Yu, M. F. Mechanochemical delivery and dynamic tracking of fluorescent quantum dots in the cytoplasm and nucleus of living cells. *Nano Lett.* **9,** 2193–2198 (2009).
40. Alivisatos, A. P., Gu, W. W. & Larabell, C. Quantum dots as cellular probes. *Annu. Rev. Biomed. Eng.* **7,** 55–76 (2005).

Acknowledgements

The authors are grateful to J. Byrd and N. Muthusamy for generously providing patient cancer cells, valuable discussions and comments. The authors thank the National Science Foundation (grant nos EEC-0425626 and EEC-0914790) and the National Institutes of Health (grant no. EB008247) for financially supporting this study. W.L. acknowledges the support from WCU Program by Korea National Research Foundation (NRF).

Author contributions

L.J.L. proposed the concept. P.E.B. and L.J.L. conceived and designed the experiment and analysis. P.E.B. performed the NEP experiments and analysed the data, with contributions from A.M. and G.P.L. regarding the optical tweezers, X. Zhang on cell culture and viability/cytotoxicity, B.Y. on siRNA and molecular beacon NEP, X.W. and Y.W. on cell culture and GFP plasmid NEP and O.H. on DCI. W.L. designed the MEP fabrication process. B.H. and H.J. performed the MEP experiments. W-C.L. and X.H. performed the simulations. L.L., K.G. and X. Zhao performed high-throughput NEP design and experiments. P.E.B., L.J.L. and G.P.L. wrote the manuscript, with input from the other authors.

Additional information

The authors declare no competing financial interests. Supplementary information accompanies this paper at www.nature.com/naturenanotechnology. Reprints and permission information is available online at http://www.nature.com/reprints. Correspondence and requests for materials should be addressed to L.J.L.